THE GEOLOGICAL SOCIETY OF AMERICA®

Subduction polarity of the Ailaoshan Ocean (eastern Paleotethys): Constraints from detrital zircon U-Pb and Hf-O isotopes for the Longtan Formation

Xiao-Ping Xia[1,†], Jian Xu[1,2], Chao Huang[1,2], Xiaoping Long[3], and Meiling Zhou[1,2]

[1]*State Key Laboratory of Isotope Geochemistry, Guangzhou Institute of Geochemistry, Chinese Academy of Sciences, Wushan, Guangzhou 510460, China*

[2]*College of Earth and Planetary Sciences, University of Chinese Academy of Sciences, Beijing 141407, China*

[3]*State Key Laboratory of Continental Dynamics, Department of Geology, Northwest University, Xi'an 710069, China*

ABSTRACT

The Paleotethys Ailaoshan Ocean separated the South China and Indochina blocks during the late Paleozoic. Uncertainty remains regarding subduction of this ocean—whether it was subducted eastward beneath the South China block or westward beneath the Indochina block. In this study, we present new detrital zircon U-Pb age, and Hf and O isotope data from the Longtan Formation, which was recognized to be deposited before the ocean closed. Our results show that the formation can be divided into three units: Unit 1 is distributed west of the suture and dominates the area; it contains major age peaks at 290–250 Ma and minor multiple old age peaks. Unit 2 consists of a minor distribution west of the suture, and it shows a dominant 250 Ma age peak; old zircons are very few or not present. Their Hf and O isotopic signatures are similar to those of unit 1. Unit 3 is distributed east of the suture and is characterized by a single distinct ca. 240 Ma age peak with almost no Precambrian zircons. We interpret that units 1 and 2 were likely deposited in a back-arc and forearc basin, respectively, and a volcanic arc developed on the eastern margin of the Indochina block, similar to the present-day northeastern Japan arc. Meanwhile, unit 3 was likely deposited in a forearc basin on the western margin of the South China block. Therefore, the Ailaoshan Ocean may undergone bipolar subduction both westward and eastward beneath the Indochina and South China blocks, respectively.

INTRODUCTION

Mainland Southeast (SE) Asia consists of an assemblage of allochthonous (micro-)continental blocks separated by a series of Tethyan sutures (Fig. 1). These blocks are generally regarded to have been derived from Gondwana and accreted to the southern margin of Eurasia during the late Paleozoic to Cenozoic (Hara et al., 2010; Metcalfe, 2013; Faure et al., 2014; Zaw et al., 2014). The northward drifting of these (micro-)continental blocks and their accretion onto the Eurasian margin consecutively opened and closed the Paleotethys, Mesotethys, and Neotethys Oceans (Rogers and Santosh, 2003; Metcalfe, 2013; Zaw et al., 2014), among which the Paleotethys is least understood, because most of its evolutionary records have been significantly altered by later deformation imposed by the Mesotethys and Neotethys (Leloup et al., 1995). Fortunately in western Yunnan (SW China), Paleotethyan ophiolites and volcanic belts are well preserved in many places (e.g., Yang et al., 2017), and they are regarded to represent the remnants of two Paleotethyan branches, i.e., the Main Paleotethyan branch (represented by the Changning-Menglian-Inthanon suture; Hara et al., 2010) and the Ailaoshan Ocean (represented by the Jingshajiang-Ailaoshan suture; Sone and Metcalfe, 2008; Zaw et al., 2014; Lai et al., 2014a). Uncertainty remains regarding whether the Ailaoshan Ocean was subducted eastward (present-day orientation) beneath the Yangtze block (part of the South China block; Duan and Hong, 1981; Xu et al., 2019a) or westward beneath the Indochina-Simao (abbreviated Indochina) block (Wang and Metcalfe, 2000; Cai and Zhang, 2009). Resolving the subduction polarity is complicated by the fact that regional late Paleozoic–Mesozoic structures were reactivated and deformed during the Cenozoic India-Asia collision (Leloup et al., 1995). Previous research on this matter mainly focused on identifying arc-related igneous rocks in the region, yet their age and geochemical interpretations have also been complicated by the overprinting magmatism and metamorphism associated with the Cenozoic India-Asia collision (Faure et al., 2014; Lai et al., 2014b).

Regional comparison of detrital zircon (a resistant mineral) U-Pb age and Hf isotopes has been increasingly adopted in tectonic reconstructions and for recognition of eroded magmatic arcs (Cawood et al., 2012; Oo et al., 2015; Xu et al., 2019b). In this paper, we first report detrital zircon U-Pb age and Hf-O isotope data for the Longtan Formation (Fig. 2), which has been widely recognized as the youngest precollisional detrital sedimentary sequence in the region. We found that different parts of the Longtan Formation contain drastically different detrital zircon populations, which represent different depositional settings (e.g., forearc and back-arc) at opposite ends of the Ailaoshan Ocean. These data lead to the conclusion that bipolar subduction of the Ailaoshan Ocean may have occurred since the Early Permian.

GEOLOGICAL BACKGROUND AND SAMPLES

Overview

The Ailaoshan belt in SW Yunnan, China (~300 km long and 20–100 km wide; Fig. 1), is located between the South China and Indochina blocks. The belt is bounded by the Amojiang-Lixianjiang fault to the west and the Red River fault to the east (Fig. 2; YNGMR, 1990). The Ailaoshan belt continues to the Jinshajiang belt to the northwest

†xpxia@gig.ac.cn

GSA Bulletin; May/June 2020; v. 132; no. 5/6; p. 987–996; https://doi.org/10.1130/B35294.1; 9 figures; 1 table; Data Repository item 2019346; published online 7 October 2019.

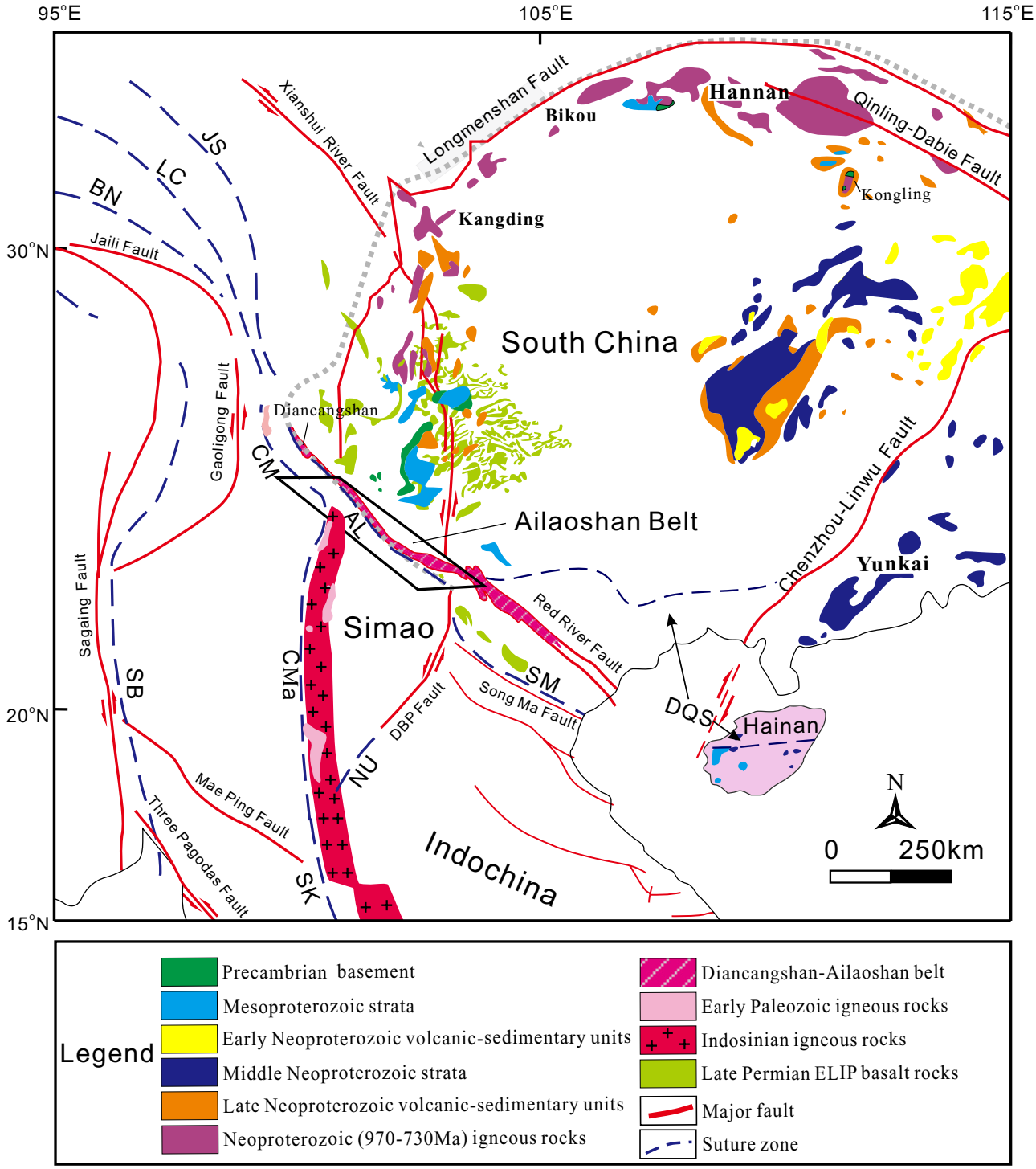

Figure 1. Tectonic map of South China and mainland SE Asia (modified from Xia et al., 2016). Abbreviations: AL—Ailaoshan; CM—Changning-Menglian; LC—Lancangjiang; ELIP—Emeishan large igneous province; JS—Jinshajiang; SM—Song Ma; DQS—Dian-Qiong Suture; NU—Nan-Uttaradit; BN—Bangong-Nujiang; SK—Sra Kaeo; SB—Shan boundary; CMa—Chiang Mai; DBP—Dian Bian Phu.

(Mo et al., 1998), whereas its southeastern extension is uncertain (Lepvrier et al., 2008; Cai and Zhang, 2009). The Ailaoshan-Tengtiaohe fault has been recognized as the suture between the South China and Indochina blocks (Xia et al., 2016), although uncertainty remains as the Lixianjiang fault (Chung et al., 1997) and an ophiolite belt (Wang et al., 2014) have also been proposed. The Ailaoshan-Tengtiaohe fault separates the Ailaoshan high-grade metamorphic belt (with South China affinity) in the east from the lower-grade

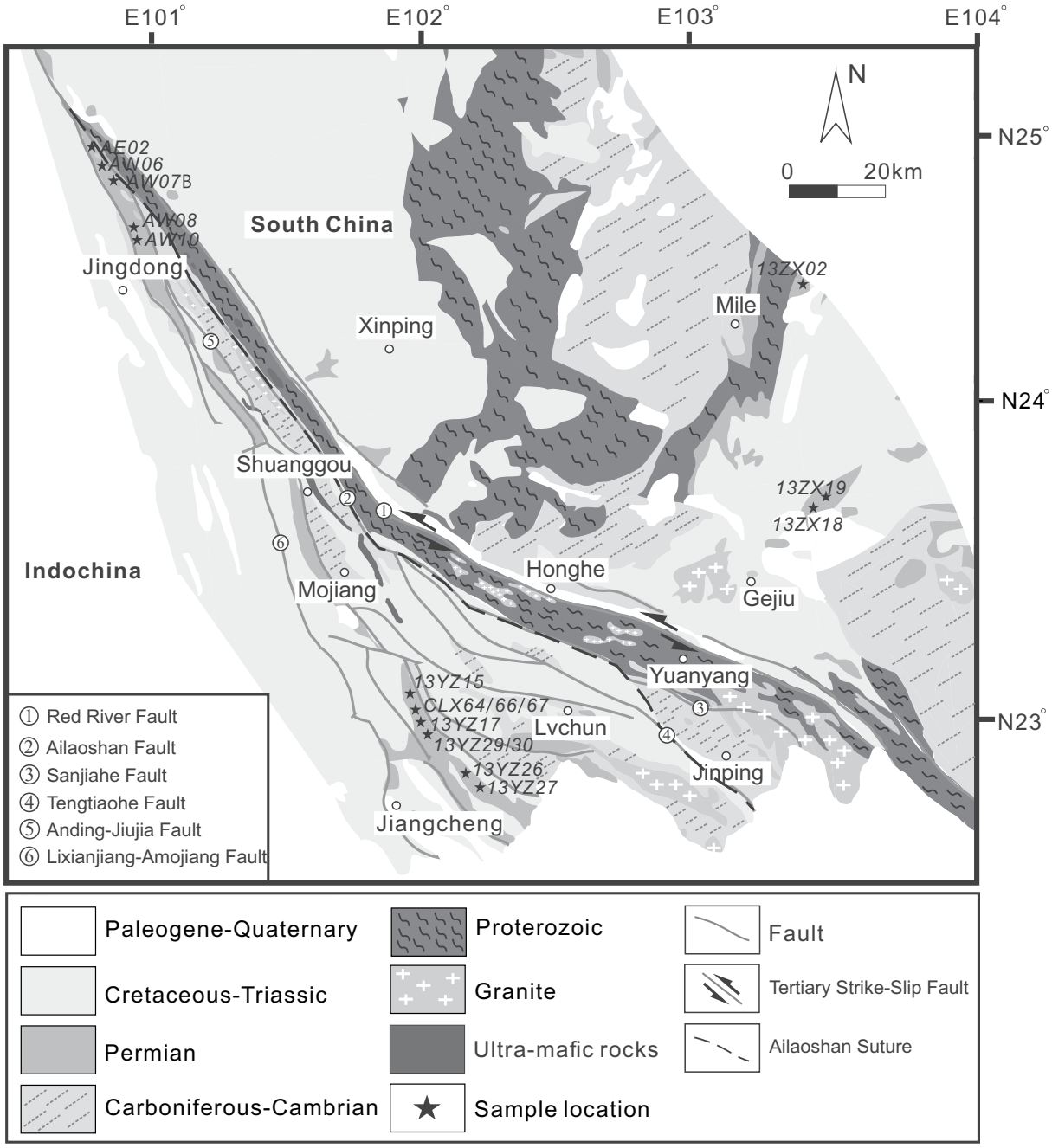

Figure 2. Geologic map showing the stratigraphic sequences and igneous rocks of the Ailaoshan area. Sample locations are indicated (modified from Wang et al., 2014; Xia et al. 2016).

greenschist-facies–metamorphosed Silurian to Triassic volcanic-sedimentary sequences and ultramafic-felsic intrusions in the west (YNGMR, 1990; Fan et al., 2010; Lai et al., 2014b). The low-grade metamorphic belt is dominated by Paleozoic marine sedimentary rocks, Triassic terrestrial sedimentary rocks, and granitoids. The Paleozoic strata consist of metamorphosed clastic sedimentary rocks. Coupled with the high-grade metamorphic belt, they were once considered to be paired metamorphic belts located at the margin of the South China block and indicated eastward subduction of the Paleo-Tethys Ailaoshan Ocean beneath the South China block (Duan and Hong, 1981). However, recent studies have identified that the low- and high-grade metamorphic belts belong to the Indochina and South China blocks, respectively (Wang et al., 2014; Xia et al., 2016).

Stratigraphy and Samples

The Longtan Formation, the focus of this study, is exposed widely throughout southern China. It is characterized by a *Gigantopteris* coal series in South China and is regarded to have been deposited in the late Early Permian, although it is not strictly synchronous in different localities. In the study area, it is distributed on both sides of the Ailaoshan suture, although the

exposure is very limited. We noted that a single formation distributed on both sides of a tectonic belt is generally not the case in most areas, and three units were identified based on the detrital zircon data in this study. Therefore, the so-called Longtan Formation in the study area should be divided into members. West of the Ailaoshan suture, the formation is mainly exposed in the Jingdong and Lvchun-Jiangcheng areas. East of the suture, the formation is mainly exposed in the Gejiu-Mile area in the western Yangtze block (Fig. 2). Sampling in this study was conducted in the Longtan Formation on both sides of the Ailaoshan suture (Figs. 2 and 3). In the western side of the suture, we collected 14 samples in the Lvchun-Jiangchen (CLX64, CLX67, CLX66, 13YZ17, 13YZ26, 13YZ27, 13YZ15, 13YZ29, and 13YZ30) and in the Jingdong (AE02, AW06, AW07, AW08, AW10) area. In the sampling area, the Longtan Formation overlies the Lower Carboniferous sequences along a parallel unconformity (Fig. 3). The lower part of the Longtan Formation consists of shale-sandstone interbeds, limestone lenses, and coal seams. The middle part of the Longtan Formation is composed mainly of feldspathic lithic sandstone interbedded with sandy shale in the north, and mainly tuff in the south. The upper part of the Longtan Formation consists of sandy shale interbedded with sandstone, limestone, and coal seams. The Changxing Formation, dominantly limestone, conformably overlies the Longtan Formation. Comparatively, there are fewer Upper Permian sedimentary rocks to the east of the Ailaoshan suture, and our three samples were collected in the Gejiu (13ZX18 and 13ZX19) and Mile (13ZX02) areas. The Longtan Formation rocks in Mile comprise mainly sandy shale, siltstone, and fine sandstone interbedded with sandy limestone, whereas those in Gejiu comprise mainly carbonaceous shale interbedded with coal seams. The Longtan Formation east of the suture is unconformably underlain by the Emeishan basalt or Upper Triassic sequences (Fig. 3). Quartz is the most abundant mineral in all the samples, and volcanic lithic clasts can be found in some samples. Detailed sample descriptions are summarized in Table 1, and thin section microphotographs are shown in Figure 4.

ANALYTICAL METHODS

Detrital zircons of each sample were separated from ~5 kg crushed samples using conventional magnetic and heavy liquid techniques, and individual grains were handpicked under a binocular microscope. In total, 200 (out of >500) zircons for each sample were randomly selected, mounted in epoxy resin, and polished to approximately half of the original thickness. The zircons were studied under transmitted and reflected light before analyses in order to avoid cracks or inclusions. Cathodoluminescence (CL) images were obtained to characterize zircon internal structure for isotope analysis spot selection (Fig. 5).

Zircon U-Pb Dating

The detrital zircon U-Pb dating was conducted using a Neptune Plus multicollector–inductively coupled plasma–mass spectrometer (MC-ICP-MS) coupled with a RESOlution M-50 193 nm laser-ablation (LA) system at the State Key Laboratory of Isotope Geochemistry, Guangzhou Institute of Geochemistry, Chinese Academy of Sciences (GIGCAS). Device configurations were described in detail by Xia et al. (2013). Laser ablation was conducted with a 24 μm or 33 μm spot size, 4 Hz frequency, and 2 J/cm^2 energy density. Helium gas was used as a carrier gas. Each spot analysis included an ~30 s blank measurement and 30 s sample data acquisition. The raw count rates of ^{202}Hg, ^{204}Pb, ^{206}Pb, ^{207}Pb, ^{208}Pb, ^{232}Th, and ^{238}U were measured. Due to the very low ^{204}Pb count and the interference from ^{204}Hg, the common Pb could not be accurately measured, and thus no common Pb correction was carried out. The U-Th-Pb ratio and the absolute U abundance were calibrated using Harvard Zircon 91500 (Wiedenbeck et al., 1995). The zircon standard Plesovice (Sláma et al., 2008) was used to monitor the analytical results. The U-Pb analyses always yielded ages within 3% of their suggested value. All age calculations and concordia diagram production were performed with Isoplot 3.0 (Ludwig, 2003).

Lu-Hf Isotope Analysis

Same as the U-Pb dating, the in situ Hf isotope analysis was carried out using the LA-MC-ICP-MS at the State Key Laboratory of Isotope Geochemistry, GIGCAS. Lu-Hf isotope measurements were conducted on the same spot or the same age domain as the U-Pb analysis recognized by CL imaging, and only those grains with concordant U-Pb ages (discordance <5%) were selected for Lu-Hf isotope analyses. The analytical conditions included 45 μm ablation spot size, 6 Hz repetition rate, ~4 J/cm^2 energy density, and a 30 s ablation time. The mass obtained for Hf isotopes was 180 ~175, 173, and 171. The measured isotope ratio of ^{176}Hf /^{177}Hf was normalized to ^{179}Hf/^{177}Hf = 0.7325 using an exponential law. The detailed data reduction procedure was reported in Xia et al. (2011). The isotope interference of ^{176}Yb and ^{176}Lu to ^{176}Hf was corrected by monitoring ^{173}Yb and ^{175}Lu, respectively. The in situ measured ^{173}Yb/^{171}Yb ratio was used for mass bias correction of Yb and Lu,

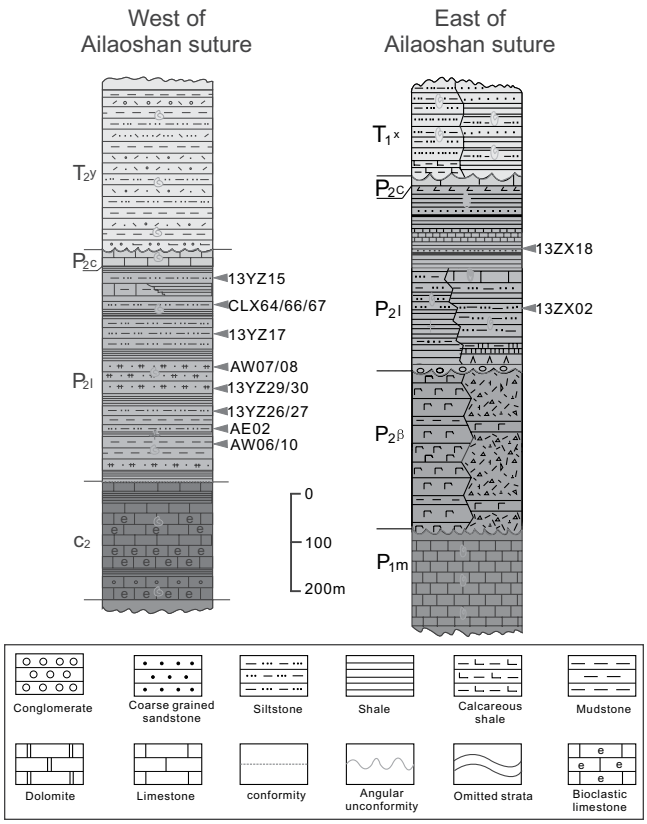

Figure 3. Simplified Carboniferous–Triassic stratigraphy at the Lvchun-Jiangcheng and Jingdong areas (west of the Ailaoshan suture) and the Gejiu-Mile area (east of the Ailaoshan suture) (modified from YNGMR, 1990). Relative stratigraphic positions of the samples in this study are indicated.

TABLE 1. SAMPLING LOCATIONS AND PETROGRAPHIC FEATURES OF THE SAMPLES

Sample	Latitude (°N)	Longitude (°E)	Lithology	Strata age	Mineral composition	Brief description
Lvchun-Jiangcheng						
CLX64	22°55.177′	101°56.468′	Mudstone	L. Permian	Quartz (30%–40%), feldspar (15%–20%), mica (15%–20%), and matrix (30%–40).	Low-grade metamorphic.
CLX66	22°51.386′	101°57.367′	Siltstone	L. Permian	Quartz (30%–40%), feldspar (15%–20%), mica (5%–10%), and matrix (30%–41).	Fine-grained, subrounded, moderately sorted.
CLX67	22°50.900′	101°56.481′	Arkose	L. Permian	Quartz (55%–65%), feldspar (25%–30%), mica (0%–5%), lithic fragments (0%–15%), and minor heavy mineral.	Medium-grained, subrounded to rounded, moderately sorted.
13YZ15	22°59.089′	101°56.501′	Lithic sandstone	L. Permian	Sedimentary and volcanic lithic clasts (60%–70%), and matrix (10%–15%).	Fine- to medium-grained, subangular to subrounded, moderately to poorly sorted.
13YZ17	22°51.377′	101°57.273′	Arkose	L. Permian	Quartz (65%–70%), feldspar (20%–25%), and lithic fragments (0%–10%).	Medium-grained, subrounded to rounded, moderately sorted.
13YZ26	22°32.174′	102°13.484′	Lithic sandstone	L. Permian	Quartz (65%–70%), feldspar (5%–10%), and lithic fragments (15%–20%).	Medium-grained, subrounded to rounded, moderately sorted.
13YZ27	22°27.400′	101°53.720′	Arkose	L. Permian	Quartz (65%–70%), feldspar (20%–25%), and lithic fragments (0%–10%).	Medium-grained, subrounded to rounded, moderately sorted.
Jingdong						
AE02	24°56.370′	100°47.470′	Quartz arenites	L. Permian	Quartz (~90%), feldspar (~5%), and minor heavy minerals.	Medium-grained, subrounded to rounded, well to moderately sorted.
AW06	24°51.429′	100°46.705′	Siltstone	L. Permian	Quartz (30%–40%), feldspar (15%–20%), mica (5%–10%), and matrix (30%–40%).	Fine-grained, subrounded, moderately sorted.
AW07	24°51.160′	100°46.101′	Lithic sandstone	L. Permian	Quartz (60%–65%), sedimentary and volcanic lithic clasts (60%–70%), and matrix (5%–10%).	Low-grade metamorphic.
AW08	24°36.127′	100°53.476′	Lithic sandstone	L. Permian	Quartz (5%–10%), sedimentary and volcanic lithic clasts (60%–70%), and matrix (10%–15%).	Fine- to medium-grained, subrounded, poorly sorted.
13YZ29	23°00.513′	101°04.223′	Lithic sandstone	L. Permian	Quartz (5%–10%), sedimentary and volcanic lithic clasts (60%–70%), and matrix (10%–15%).	Fine- to medium-grained, subrounded, poorly sorted.
AW10	24°34.701′	100°54.765′	Quartz arenites	L. Permian	Quartz (~90%), feldspar (~5%), and minor heavy minerals.	Medium-grained, subrounded to rounded, well to moderately sorted.
13YZ30	23°07.659′	101°01.607′	Lithic sandstone	L. Permian	Quartz (5%–10%), sedimentary and volcanic lithic clasts (60%–70%), and matrix (10%–15%).	Fine- to medium-grained, subrounded, poorly sorted.
Gejiu						
13ZX18	23°37.936′	103°24.062′	Siltstone	L. Permian	Quartz (80%–85%), feldspar (0%–10%), and matrix (0%–10%).	Medium-grained, subrounded to rounded, well to moderately sorted.
13ZX19	23°40.561′	103°27.930′	Siltstone	L. Permian	Quartz (~80%), feldspar (~5%), and matrix (5%–10%).	Medium-grained, subrounded to rounded, well to moderately sorted.
Mile						
13ZX02	24°22.162′	103°24.738′	Siltstone	L. Permian	Quartz (30%–40%), feldspar (15%–20%), mica (5%–10%), and lithic fragments (30%–40%).	Fine-grained, subrounded, moderately sorted.

since these two elements have similar physicochemical properties. The ratios used for the correction were 0.7963 for $^{176}Yb/^{173}Yb$ and 0.02655 for $^{176}Lu/^{175}Lu$ (Vervoort et al., 2004). The zircon standard Penglai (Li et al., 2010) was analyzed twice every hour to check the reliability of the method. The results were always within ± 1.5μ Hf of the recommended values. The decay constant of 1.867×10^{-11}/yr for ^{176}Lu (Scherer et al., 2001), the current chondrite values of $^{176}Hf/^{177}Hf = 0.282785$ and $^{176}Lu/^{177}Hf = 0.0336$ (Bouvier et al., 2008), and the zircon age obtained by the previous U-Pb dating were used to calculate $\varepsilon_{Hf(t)}$. Two types of Hf-model ages, T_{DM} and T^{C}_{DM}, were calculated from the U-Pb age and the Lu-Hf isotope measurements for zircons. The single-stage model age (T_{DM}), representing the minimum age of the zircon parent magma, was calculated relative to the depleted mantle with the current values $(^{176}Lu/^{177}Hf)_{DM} = 0.0384$ and $(^{176}Hf/^{177}Hf)_{DM} = 0.28325$ (Griffin et al., 2000). The two-stage model age (T^{C}_{DM}) was calculated with the assumption that the zircon parent magma was produced by the average continental crust ($^{176}Lu/^{177}Hf = 0.015$) derived from a depleted mantle source, which we consider to be a more realistic age estimation of the magma source.

Oxygen Isotope Analysis

Zircon oxygen isotopes were measured using the CAMECA IMS1280-HR secondary ion mass spectrometer (SIMS) at the State Key Laboratory of Isotope Geochemistry, GIGCAS. The detailed procedures were same as those described by Yang et al. (2018). The $^{133}Cs+$ primary ion beam with an intensity of ~2 nA was accelerated at 10 kV and focused on an area of Φ 10 μm on the sample surface, and the size of the analysis spot was ~20 μm in diameter (10 μm beam diameter + 10 μm raster). Two off-axis Faraday cups were used to measure oxygen isotopes in a multicollector mode. The total analysis time for each spot was ~3.5 min, including 30 s of presputtering, 120 s of secondary beam automatic tuning, and 64 s of analysis. The oxygen isotope data were corrected for the instrument mass fraction (IMF) using the Penglai zircon standard ($\delta^{18}O_{VSMOW} = 5.3‰$, where VSMOW is Vienna standard mean ocean water; Li et al., 2010). The internal precision of a single analysis is usually ~0.1‰ (1σ) for the $^{18}O/^{16}O$ ratio. The external precision of the point-to-point reproducibility measurement by repeating the Penglai standard was 0.30‰ (2σ, $n = 24$) for data evaluation. In this study, a $\delta^{18}O$ weighted average of 5.60‰ ± 0.10‰ (2σ) was obtained for

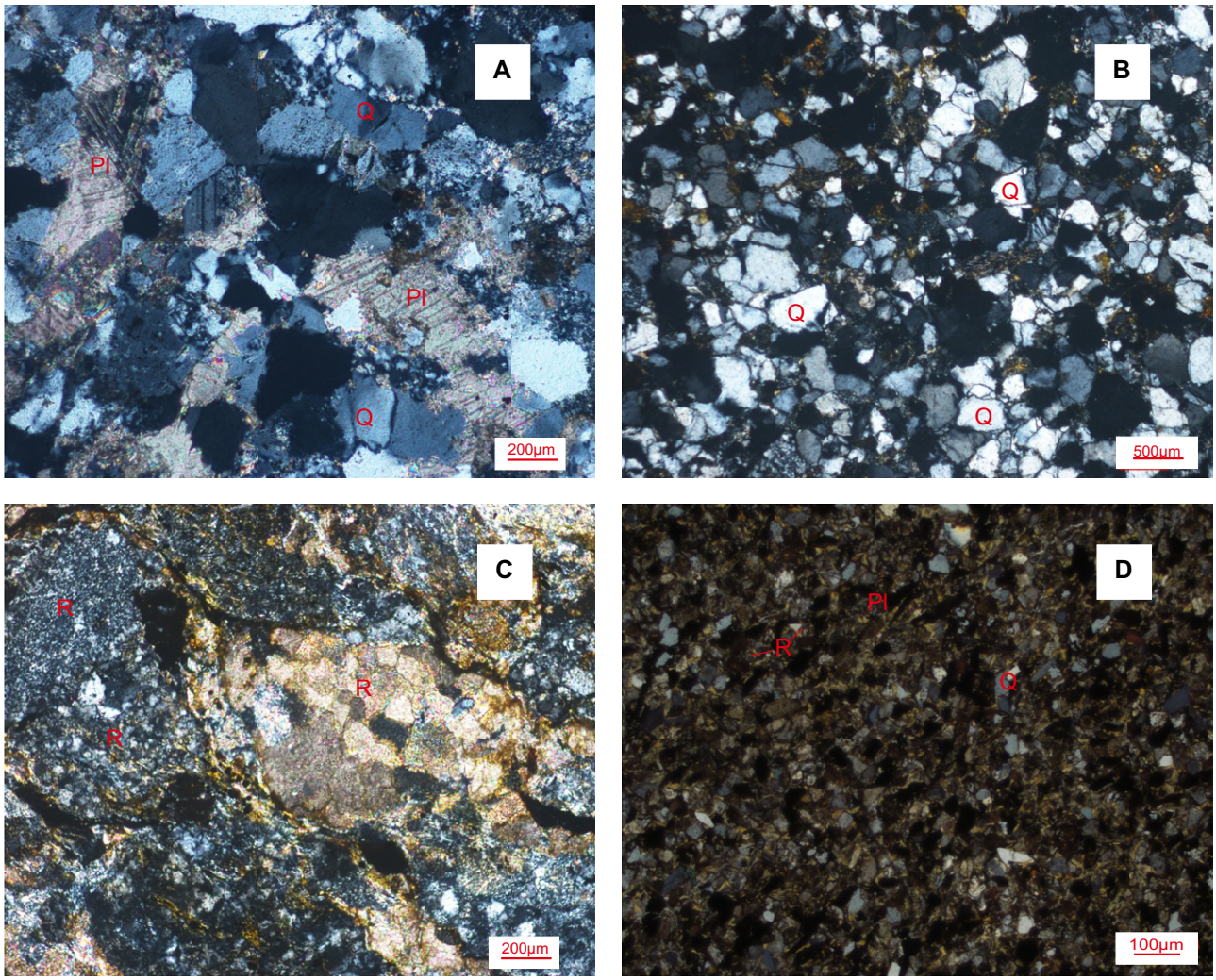

Figure 4. Thin section microphotographs of the Longtan samples (cross-polar). (A) Sample CLX67 (arkose). (B) Sample AW10 (quartz arenite). (C) Sample AW07 (lithic sandstone); (D) Sample 13ZX19 (siltstone). Abbreviations for minerals: Q—quartz; Pl—plagioclase; R—rock fragments.

15 measurements of the Qinghu zircon standard, which is within analytical error of the recommended value (5.4‰ ± 0.2‰; Li et al., 2013).

RESULTS

LA-MC-ICP-MS detrital zircon U-Pb age data for the 17 analyzed samples are listed in Table DR1 and illustrated in Figures DR1 and DR2 as supplementary materials.[1] The age probability plots (Fig. DR2) were constructed based on their $^{207}Pb/^{206}Pb$ ages when their ages were older than 1000 Ma; otherwise, their $^{238}U/^{206}Pb$ ages were used, which provide a more reliable zircon age estimation. Zircons were mostly colorless and transparent. Most of the zircons showed clear oscillatory CL zoning without inherited cores or overgrowth rims and had high Th/U ratios (Fig. 5; Table DR1), indicating their magmatic origin. The detrital zircon Hf-O isotope data are listed in Tables DR2 and DR3 as supplementary materials (see footnote 1). According to their detrital zircon age and Hf-O isotope features, the sedimentary rock samples can be divided into three units.

Unit 1: Multimodal Zircon Populations

Unit 1 clastic rock samples are mainly lithic-feldspar sandstone (CLX64, CLX66, CLX67, 13YZ17, 13YZ26, 13YZ27, AW06; Fig. 4A) with minor quartz arenite (AE02, AW10; Fig. 4B). Detrital zircons from the former are more angular than those from the latter (Fig. 5). These rock samples contain detrital zircon ages up to 3559 Ma, with major age peaks at 290–250 Ma and minor peaks at 420 Ma, 800 Ma, and 1800 Ma (Fig. 6; Figs. DR1–DR2 [footnote 1]). For the majority of the zircons (i.e., those 290–250 Ma), the $\varepsilon_{Hf(t)}$ values are both positive and negative (–19.88 to + 16.79; Fig. 7; Table DR2 [footnote 1]), with $\delta^{18}O$ values from + 5‰ to + 11‰ (Fig. 8; Table DR3 [footnote 1]).

Unit 2: Unimodal Zircon Population (Peak at 250 Ma)

Unit 2 clastic rock samples comprise mainly lithic sandstone (AW07, AW08, 13YZ15, 13YZ29, and 13YZ30; Fig. 4C), and the lithic fragments are mainly volcanic, indicating a proximal volcanic provenance. The zircons are all euhedral, and their age spectrum shows a distinct single peak at 250 Ma and contains few older zircons (Fig. 6; Fig. DR2 [footnote 1]). The $\varepsilon_{Hf(t)}$ values from unit 2 zircons are also both positive

[1]GSA Data Repository item 2019346, Tables DR1–DR3, and Figures DR1 and DR2, is available at http://www.geosociety.org/datarepository/2019 or by request to editing@geosociety.org.

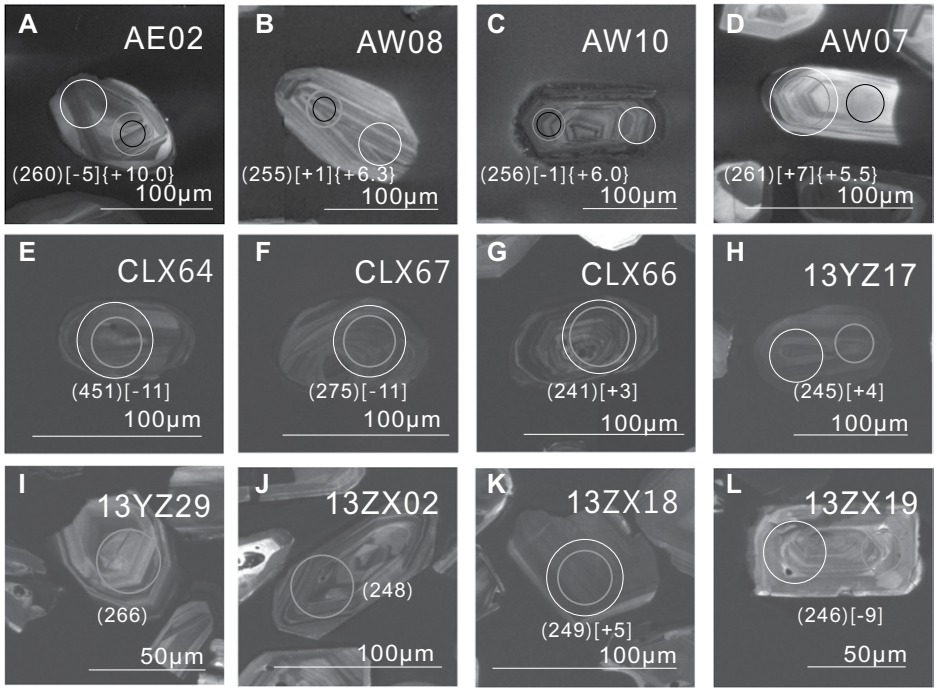

Figure 5. Representative zircon cathodoluminescence (CL) images from the Longtan sedimentary rocks. Analytical spots and data for U-Pb (gray cycle), Lu-Hf (white cycle), and O (black cycle) isotopes are shown. Numbers near the analytical spots are the U-Pb ages (within parentheses, Ma), $\varepsilon_{Hf(t)}$ values [within square brackets], and $\delta^{18}O$ values {within braces, ‰}.

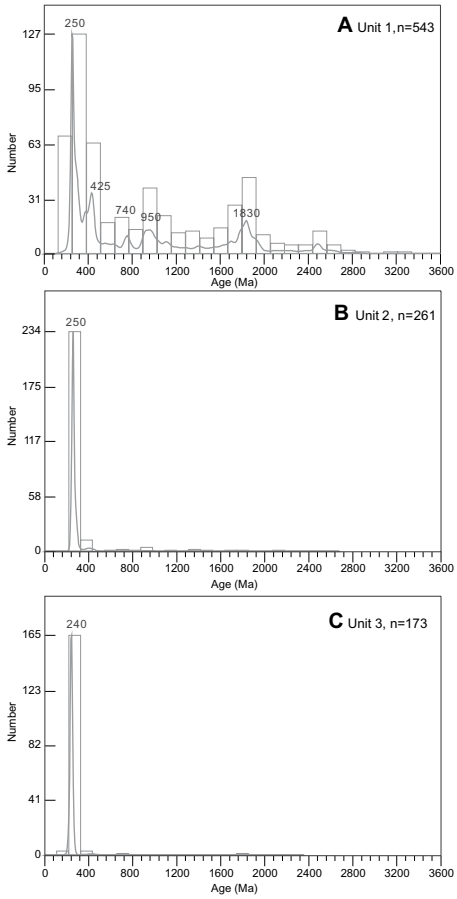

Figure 6. Detrital zircon U-Pb age probability plot for the three units of the Longtan Formation.

and negative (–29.19 to + 8.97; Fig. 7; Table DR2 [footnote 1]). For those zircons with an age of ca. 250 Ma, their $\varepsilon_{Hf(t)}$ values are similar to those from unit 1, although a few grains from unit 1 had higher $\varepsilon_{Hf(t)}$ up to depleted mantle values (Fig. 7). The $\delta^{18}O$ values of unit 2 zircons (+4‰ to + 9‰) are similar to those of unit 1 (+5‰ to + 11‰; Fig. 8; Table DR3 [footnote 1]).

Unit 3: Unimodal Zircon Population (Peak at 240 Ma)

Unit 3 samples were all from the eastern side of the Ailaoshan suture and consisted of moderately sorted siltstone (13ZX02, 13ZX18, and 13ZX19; Fig. 4D). The zircons ranged from euhedral to anhedral (Figs. 5I and 5K), with ages ranging ca. 744–229 Ma (peak at 240 Ma; Fig. 6; Figs. DR1–DR2 [footnote 1]). The $\varepsilon_{Hf(t)}$ values ranged from negative to positive (–15.27 to + 8.96; Fig. 7; Table DR3 [footnote 1]). No oxygen isotope data were obtained for unit 3 zircons.

DISCUSSION

Permian Volcanic Arc in the Eastern Margin of the Indochina Block

Sedimentary basins in convergent margins are characterized by a higher proportion of detrital zircons with ages close to the sediment deposition age, which is different from collisional/extensional-related sedimentary basins, where the majority of the detrital zircons are much older than the sediment deposition age (Fedo et al., 2003; Escayola et al., 2007). In addition, forearc basins are distinct in terms of their unimodal detrital zircon population with ages close to the sediment deposition age (DeGraaff-Surpless et al., 2002; Wu et al., 2010; Decou et al., 2013).

Although the suture line between the South China and Indochina blocks has been proposed to be the Lixianjiang fault (Chung et al., 1997), recent research has relocated it to be the ophiolite belt (Wang et al., 2014) or its adjacent Ailaoshan-Tengtiaohe fault (Xia et al., 2016). Unit 1 and 2 samples were collected from west of the both the ophiolite belt and the Ailaoshan-Tengtiaohe fault, and so they represent the sediments deposited at the eastern margin of the Indochina block. Each sample yielded an average of 60 concordant ages (>90%). Most of the 290–250 Ma zircons in this study were subhedral, implying medium-distance transportation. Considering that samples 13YZ15, 13YZ26, 13YZ29, 13YZ30, AW07, and AW08 contain variable portions of lithic clasts, some of which are obviously volcanic clasts (Table 1), consistent with the interpretation that sediments were sourced from a proximal arc system, we propose that the western Ailaoshan volcanic arcs may represent a likely detrital source for these sedimentary rock samples. Permian arc-related igneous rocks have been reported in the Taizhong-Lixianjiang (Wei and Shen, 1997; Liu et al., 2011) and Wusu-Yaxuanqiao (Fan et al., 2010) areas on the western margin of the Indochina-Simao block. The Taizhong-Lixianjiang arc-related igneous rocks were dated to be Middle Permian to Triassic. The Wusu and Yaxuanqiao volcanic rocks, which show an arc or mature back-arc basin (mid-ocean-ridge basalt [MORB]–like) geochemical affinity, were dated to be Permian (288–265 Ma). These rocks suggest continuous Middle Permian to Late Triassic subduction along the eastern margin of the Indochina block (Liu et al., 2011).

As mentioned above, unit 2 samples have a unimodal detrital zircon age distribution. They were likely deposited in a forearc basin (DeGraaff-Surpless et al., 2002; Wu et al., 2010; Decou et al., 2013), with their detritus mainly derived from the local Taizhong-Lixianjiang volcanic arc system (Fig. 9A). Compared with unit 2, unit 1 samples contain larger amounts of older zircons (minor peaks at 430–400 Ma, 950 Ma, and 1830 Ma; Fig. 6). As noted by previous studies, Ordovician–Silurian mafic-felsic rocks are extensively

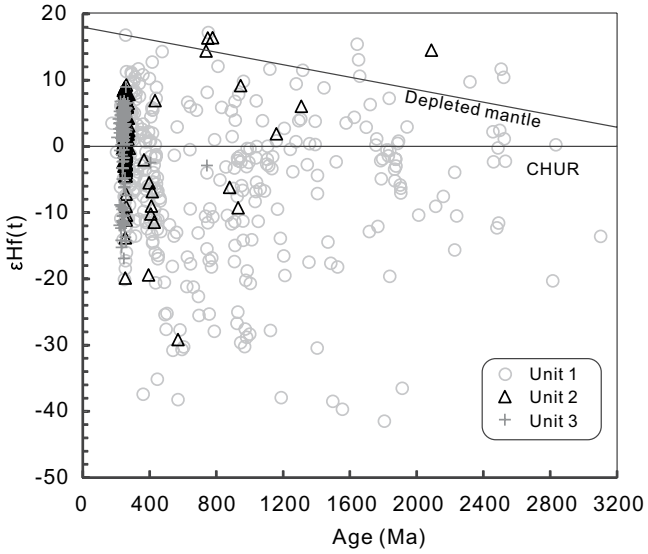

Figure 7. Plot of $\varepsilon_{Hf(t)}$ vs. age (Ma) for the detrital zircons from the Longtan Formation. Hf-isotope evolution line for depleted mantle follows Griffin et al. (2000). CHUR—chondritic uniform reservoir.

exposed on the western edge of the Indochina-Simao block (e.g., Lehmann et al., 2013), and in central Vietnam (e.g., Tran et al., 2014). Although fewer 1000–900 Ma igneous rocks have been recognized in the Indochina block, previous detrital zircon studies on Silurian–Triassic and modern river sediments from this block and inherited-xenocrystic zircons from a Triassic granite have indicated pronounced age peaks at ca. 439, 957, and 1847 Ma, and their Hf isotope data are similar to our results (Burrett et al., 2014; Wang et al., 2014; Xia et al., 2016). Therefore, Precambrian zircons were possibly sourced from recycled older sediments. Considering that the sediments from unit 1 show a higher textural maturity than their unit 2 counterparts (Figs. 4 and 5), we suggest that the unit 1 detritus may have been derived mainly from the Taizhong-Lixianjiang volcanic arcs, with minor contributions from the Indochina block (Usuki et al., 2013; Burrett et al., 2014); this points to a probable back-arc basin setting for the sediment deposition (Fig. 9A).

Middle Triassic Volcanic Arc in the Western Margin of the South China Block

Unit 3 samples (13ZX02, 13ZX18, and 13ZX19) all come from east of the Ailaoshan suture. Most of the detrital zircons were euhedral to subhedral, indicating a proximal provenance. The unimodal detrital zircon age population (ca. 240 Ma; Fig. 6) suggests a probable forearc basin setting (Cawood et al., 2012). Because all three samples were subrounded to rounded and well to moderately sorted, and lithic fragments occurred in the samples, we favor the interpretation that they were deposited in an unstable hydrodynamic environment with a proximal arc source, not a long-distance source. Although coeval arc-related igneous rocks have not been reported in the western margin of the South China block, our recent work has identified some Middle Triassic (ca. 237–235 Ma) gabbroic diorites and granodiorites in the Ailaoshan high-grade metamorphic belt, which have arc affinity and may represent relict of a Triassic island arc providing detritus to unit 3. Therefore, it is possible that the volcanic arc was mostly eroded, buried, or magmatically recycled, probably during the Cenozoic India-Asia collision and postcollisional extension.

Considering that the sampling area of this unit (Gejiu and Mile) is very close to (or within) the Emeishan large igneous province, another possibility arises that unit 3 sediments could have incorporated the Emeishan large igneous province–derived zircons, such as zircons from 238 to 260 Ma A-type granites and rhyolitic tuff (Xu et al., 2008). Although the age range overlaps with our unit 3 zircons, most granitoids associated with the Emeishan large igneous province have an age peak at ca. 260 Ma, which is significantly older than that for our unit 3 zircon. Also, most of the Emeishan large igneous province–derived ca. 260 Ma zircons show positive $\varepsilon_{Hf(t)}$ values (Xu et al., 2008), which are obviously different from unit 3 zircons of this study. Although ca. 238 Ma rhyolitic tuff has a very consistent age and similar $\varepsilon_{Hf(t)}$ values to those of our unit 3 zircons, there are very few occurrences in the Emeishan large igneous province, and it cannot be the source of unit 3. As stated by Xu et al. (2008), it is not easy to evaluate whether these rhyolitic tuffs were related to the Emeishan large igneous province or not. Circa 250 Ma volcanic ash beds are widely distributed in South China and have also been interpreted to be a result of the closure of the Paleo-Tethys Ocean (Yang et al., 2012; Gao et al., 2015), although different opinions exist (Xu et al., 2007).

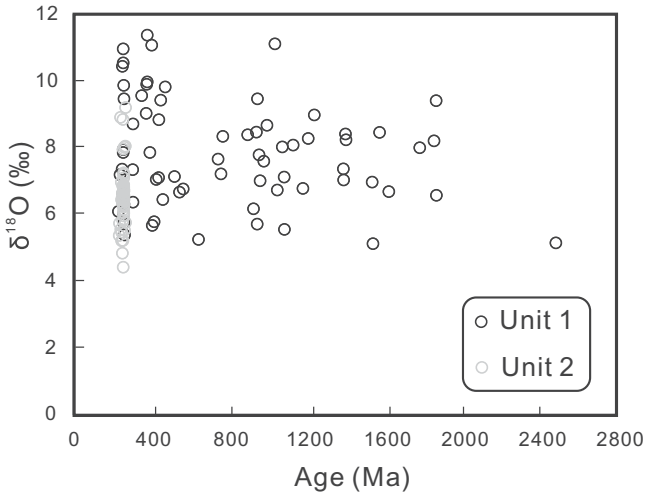

Figure 8. $\delta^{18}O$ vs. age (Ma) plot for the detrital zircons from the Longtan Formation.

Bipolar Subduction of the Ailaoshan Paleotethys Branch

As mentioned above, the subduction polarity of the Ailaoshan Ocean remains controversial, i.e., west-dipping beneath Indochina or east-dipping beneath South China. Workers who favor the former have suggested that the Taizhong-Lixianjiang volcanic arcs are evidence for subduction beneath the Indochina block (Wei and Shen, 1997). In contrast, workers who favor the latter suggest that the paired metamorphic belts in eastern Ailaoshan (Duan and Hong, 1981), with the medium- to high-temperature belt located northeast of the low-temperature and medium- to high-pressure belt, indicate a northeast-dipping subduction.

Due to the lack of direct arc-related magmatic evidence on the western margin of the South China block, and the structural disruption imposed by the Cenozoic India-Asia collision, the east-dipping hypothesis has been less favored in the literature. Our previous detrital zircon U-Pb data on the Middle Triassic sequence in the suture showed a similar U-Pb age pattern as

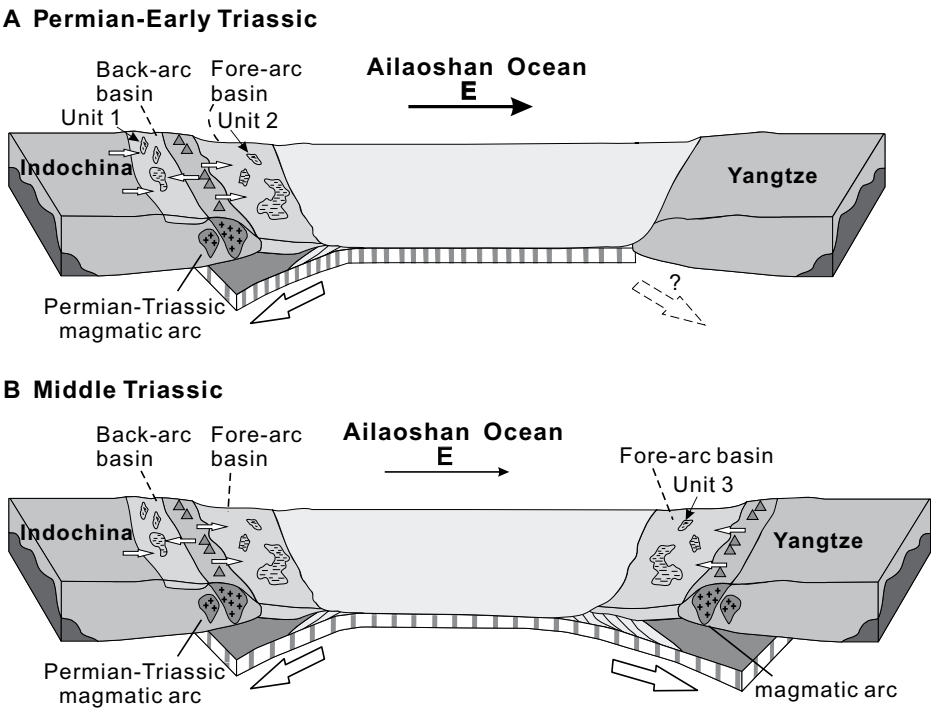

Figure 9. Schematic diagram of the evolution of the Ailaoshan Ocean from Early Permian to Middle Triassic.

that of the Longtan Formation east of the suture, which also indicates that a possible arc system developed along the west margin of the South China block (Xu et al., 2019b). However, it can be argued that the Middle Triassic sequence was possibly deposited after the ocean closed, and those detrital zircons may have come from the Taizhong-Lixianjiang arc, developed along the east margin of the Indochina block. Therefore, this study presents the first evidence on the probable existence of an eroded arc in western South China. The distinct ca. 240 Ma detrital zircon age peak suggests that this subduction-related arc magmatism was likely active during the Middle Triassic (Fig. 9B), consistent with some suggestions that the Ailaoshan Ocean was completely closed by the Late Triassic (Huang and Opdyke, 2016; Xu et al., 2019c). Recent studies have proposed that southeast (SE) Guangxi was possibly a part of the eastern Paleo-Tethys, and Permian to Triassic igneous rocks in the area were a product of east (north) subduction of the east Paleo-Tethys Ocean (e.g., Li et al., 2016), although some previous studies assigned them to be a product of westward subduction of the Pacific block (Li et al., 2006). Detrital zircon provenance analyses for the Permian to Triassic strata in the area also indicated a Permian arc system associated with the eastward subduction of the east Paleo-Tethys Ocean (e.g., Yang et al., 2012; Hou et al., 2017). Therefore, the Ailaoshan Ocean may have started its eastward subduction in the Permian (Fig. 9A). Thus, our new results and previous data from SE Guangxi consistently indicate that east (north) subduction of the Paleo-Tethys Ocean in southwest China did exist, and more attention must be paid in any attempt to reconstruct the Paleozoic to Mesozoic tectonic evolution of the South China block in the future, which has been mostly ignored in previous studies.

CONCLUSIONS

Our detrital zircon U-Pb age and Hf-O isotope data for the Longtan Formation indicated that it can be divided into three units: Unit 1 is distributed to the west of the suture and dominates the area, and it contains major age peaks at 290–250 Ma and minor multiple old age peaks. Unit 2 consists of a minor distribution west of the suture, and it shows a dominant 250 Ma age peak; old zircons are very few or not present. Hf and O isotopic signatures of unit 2 samples are similar to those of unit 1. Unit 3 is distributed to the east of the suture and is characterized by a single distinct ca. 240 Ma age peak with almost no Precambrian zircons. Units 1 and 2 were likely deposited in a back-arc and forearc basin, respectively, and a volcanic arc developed on the eastern margin of the Indochina block, similar to the present-day northeastern Japan arc. Meanwhile, unit 3 was likely deposited in a forearc basin in the western margin of the South China block. Therefore, the Ailaoshan Ocean may have undergone bipolar subduction both westward and eastward beneath the Indochina and South China blocks, respectively.

ACKNOWLEDGMENTS

This study was financially supported by the National Key Research and Development Program of China (2016YFC0600407) and the National Natural Science Foundation of China (project no. 41173007 and no. 41673010) to Xiaoping Xia. Yongfeng Cai is thanked for his assistance in the field trip. This is contribution No.IS-2737 to the Guangzhou Institute of Geochemistry, Chinese Academy of Sciences.

REFERENCES CITED

Bouvier, A., Vervoort, J.D., and Patchett, P.J., 2008, The Lu-Hf and Sm-Nd isotopic composition of CHUR: Constraints from unequilibrated chondrites and implications for the bulk composition of terrestrial planets: Earth and Planetary Science Letters, v. 273, no. 1-2, p. 48–57, https://doi.org/10.1016/j.epsl.2008.06.010.

Burrett, C., Zaw, K., Meffre, S., Lai, C.K., Khositanont, S., Chaodumrong, P., Udchachon, M., Ekins, S., and Halpin, J., 2014, The configuration of Greater Gondwana—Evidence from LA ICPMS, U-Pb geochronology of detrital zircons from the Palaeozoic and Mesozoic of Southeast Asia and China: Gondwana Research, v. 26, no. 1, p. 31–51, https://doi.org/10.1016/j.gr.2013.05.020.

Cai, J.-X., and Zhang, K.-J., 2009, A new model for the Indochina and South China collision during the Late Permian to the Middle Triassic: Tectonophysics, v. 467, no. 1-4, p. 35–43, https://doi.org/10.1016/j.tecto.2008.12.003.

Cawood, P.A., Hawkesworth, C.J., and Dhuime, B., 2012, Detrital zircon record and tectonic setting: Geology, v. 40, no. 10, p. 875–878, https://doi.org/10.1130/G32945.1.

Chung, S.-L., Lee, T.-Y., Lo, C.-H., Wang, P.-L., Chen, C.-Y., Yem, N.T., Hoa, T.T., and Genyao, W., 1997, Intraplate extension prior to continental extrusion along the Ailao Shan–Red River shear zone: Geology, v. 25, p. 311–314, https://doi.org/10.1130/0091-7613(1997)025<0311:IEPTCE>2.3.CO;2.

Decou, A., Eynatten, H.V., Dunkl, I., Frei, D., and Wörner, G., 2013, Late Eocene to early Miocene Andean uplift inferred from detrital zircon fission track and U-Pb dating of Cenozoic forearc sediments (15–18°S): Journal of South American Earth Sciences, v. 45, p. 6–23, https://doi.org/10.1016/j.jsames.2013.02.003.

DeGraaff-Surpless, K., Graham, S.A., Wooden, J.L., and Mcwilliams, M.O., 2002, Detrital zircon provenance analysis of the Great Valley Group, California: Evolution of an arc-forearc system: Geological Society of America Bulletin, v. 114, no. 12, p. 1564–1580, https://doi.org/10.1130/0016-7606(2002)114<1564:DZPAOT>2.0.CO;2.

Duan, X., and Hong, Z., 1981, The Ailaoshan-Tengtiaohe fracture—The subduction zone of an ancient plate: Acta Geologica Sinica, v. 55, no. 4, p. 258–266.

Escayola, M.P., Pimentel, M.M., and Armstrong, R., 2007, Neoproterozoic backarc basin: Sensitive high-resolution ion microprobe U-Pb and Sm-Nd isotopic evidence from the Eastern Pampean Ranges, Argentina: Geology, v. 35, no. 6, p. 495–498, https://doi.org/10.1130/G23549A.1.

Fan, W., Yuejun, W., Aimei, Z., Feifei, Z., and Yuzhi, Z., 2010, Permian arc–back-arc basin development along the Ailaoshan tectonic zone: Geochemical, isotopic and geochronological evidence from the Mojiang volcanic rocks, southwest China: Lithos, v. 119, no. 3-4, p. 553–568, https://doi.org/10.1016/j.lithos.2010.08.010.

Faure, M., Lepvrier, C., Nguyen, V.V., Vu, T.V., Lin, W., and Chen, Z., 2014, The South China block–Indochina collision: Where, when, and how?: Journal of Asian Earth Sciences, v. 79, p. 260–274, https://doi.org/10.1016/j.jseaes.2013.09.022.

Fedo, C.M., Sircombe, K.N., and Rainbird, R.H., 2003, Detrital zircon analysis of the sedimentary record: Reviews in Mineralogy and Geochemistry, v. 53, no. 1, p. 277–303, https://doi.org/10.2113/0530277.

Gao, Q., Chen, Z.-Q., Zhang, N., Griffin, W.L., Xia, W., Wang, G., Jiang, T., Xia, X., and O'Reilly, S.Y., 2015, Ages, trace elements and Hf-isotopic compositions of zircons from claystones around the Permian-Triassic boundary in the Zunyi section, South China: Implications for nature and tectonic setting of the volcanism: Journal of Earth Science, v. 26, no. 6, p. 872–882, https://doi.org/10.1007/s12583-015-0589-9.

Griffin, W., Pearson, N., Belousova, E., Jackson, S., Van Achterbergh, E., O'Reilly, S.Y., and Shee, S., 2000, The Hf isotope composition of cratonic mantle: LAM-MC-ICPMS analysis of zircon megacrysts in kimberlites: Geochimica et Cosmochimica Acta, v. 64, no. 1, p. 133–147, https://doi.org/10.1016/S0016-7037(99)00343-9.

Hara, H., Kurihara, T., Kuroda, J., Adachi, Y., Kurita, H., Wakita, K., Hisada, K.-i., Charusiri, P., Charoentitirat, T., and Chaodumrong, P., 2010, Geological and geochemical aspects of a Devonian siliceous succession in northern Thailand: Implications for the opening of the Paleo-Tethys: Palaeogeography, Palaeoclimatology, Palaeoecology, v. 297, no. 2, p. 452–464, https://doi.org/10.1016/j.palaeo.2010.08.029.

Hou, Y.-l., Zhong, Y.-t., Xu, Y.-g., and He, B., 2017, The provenance of Late Permian karstic bauxite deposits in SW China, constrained by the geochemistry of interbedded clastic rocks, and U-Pb-Hf-O isotopes of detrital zircons: Lithos, v. 278–281, p. 240–254, https://doi.org/10.1016/j.lithos.2017.01.013.

Huang, K., and Opdyke, N. D., 2016, Paleomagnetism of the Upper Triassic rocks from south of the Ailaoshan suture and the timing of the amalgamation between the South China and the Indochina blocks: Journal of Asian Earth Sciences, v. 119, p. 118–127, https://doi.org/10.1016/j.jseaes.2015.12.005.

Lai, C. K., Meffre, S., Crawford, A. J., Zaw, K., Xue, C. D., and Halpin, J. A., 2014a, The western Ailaoshan volcanic belts and their SE Asia connection: A new tectonic model for the eastern Indochina block: Gondwana Research, v. 26, no. 1, p. 52–74, https://doi.org/10.1016/J.Gr.2013.03.003.

Lai, C.K., Meffre, S., Crawford, A.J., Zaw, K., Halpin, J.A., Xue, C.D., and Salam, A., 2014b, The Central Ailaoshan ophiolite and modern analogs: Gondwana Research, v. 26, no. 1, p. 75–88, https://doi.org/10.1016/j.gr.2013.03.004.

Lehmann, B., Zhao, X., Zhou, M., Du, A., Mao, J., Zeng, P., Henjes-Kunst, F., and Heppe, K., 2013, Mid-Silurian back-arc spreading at the northeastern margin of Gondwana: The Dapingzhang dacite-hosted massive sulfide deposit, Lancangjiang zone, southwestern Yunnan, China: Gondwana Research, v. 24, p. 648–663, https://doi.org/10.1016/j.gr.2012.12.018.

Leloup, P.H., Lacassin, R., Tapponnier, P., Schärer, U., Zhong, D., Liu, X., Zhang, L., Ji, S., and Trinh, P.T., 1995, The Ailao Shan–Red River shear zone (Yunnan, China), Tertiary transform boundary of Indochina: Tectonophysics, v. 251, no. 1, p. 3–84, https://doi.org/10.1016/0040-1951(95)00070-4.

Lepvrier, C., Van Vuong, N., Maluski, H., Truong Thi, P., and Van Vu, T., 2008, Indosinian tectonics in Vietnam: Comptes Rendus Geoscience, v. 340, no. 2-3, p. 94–111, https://doi.org/10.1016/j.crte.2007.10.005.

Li, X.H., Li, Z.X., Li, W.X., and Wang, Y., 2006, Initiation of the Indosinian orogeny in South China: Evidence for a Permian magmatic arc on Hainan Island: The Journal of Geology, v. 114, no. 3, p. 341–353, https://doi.org/10.1086/501222.

Li, X.H., Long, W.G., Li, Q.L., Liu, Y., Zheng, Y.F., Yang, Y.H., Chamberlain, K.R., Wan, D.F., Guo, C.H., and Wang, X.C., 2010, Penglai zircon megacrysts: A potential new working reference material for microbeam determination of Hf-O isotopes and U-Pb age: Geostandards and Geoanalytical Research, v. 34, no. 2, p. 117–134, https://doi.org/10.1111/j.1751-908X.2010.00036.x.

Li, X.H., Tang, G., Gong, B., Yang, Y.H., Hou, K.J., Hu, Z., Li, Q., Liu, Y., and Li, W., 2013, Qinghu zircon: A working reference for microbeam analysis of U-Pb age and Hf and O isotopes: Chinese Science Bulletin, v. 58, no. 36, p. 4647–4654, https://doi.org/10.1007/s11434-013-5932-x.

Li, Y.J., Wei, J.H., Santosh, M., Tan, J., Fu, L.B., and Zhao, S.Q., 2016, Geochronology and petrogenesis of Middle Permian S-type granitoid in southeastern Guangxi Province, South China: Implications for closure of the eastern Paleo-Tethys: Tectonophysics, v. 682, p. 1–16, https://doi.org/10.1016/j.tecto.2016.05.048.

Liu, C., Deng, J., Liu, J., and Shi, Y., 2011, Characteristics of volcanic rocks from Late Permian to Early Triassic in Ailaoshan tectono-magmatic belt and implications for tectonic settings: Acta Petrologica Sinica (Yanshi Xuebao), v. 27, no. 12, p. 3590–3602.

Ludwig, K.R., 2003, User's Manual for Isoplot 3.00: A Geochronological Toolkit for Microsoft Excel: Berkeley Geochronology Center Special Publication 4, 70 p.

Metcalfe, I., 2013, Gondwana dispersion and Asian accretion: Tectonic and palaeogeographic evolution of eastern Tethys: Journal of Asian Earth Sciences, v. 66, p. 1–33, https://doi.org/10.1016/j.jseaes.2012.12.020.

Mo, X., Shen, S., Zhu, Q., Xu, T., Wei, Q., Tan, J., Zhang, S., and Cheng, H., 1998, Volcanics—Ophiolite and Mineralization of Middle-Southern Part in Sanjiang Area of Southwestern China: Beijing, Geological Publishing House [in Chinese with English abstract], 128 p.

Oo, K.L., Zaw, K., Meffre, S., Myitta, Aung, D.W., and Lai, C.K., 2015, Provenance of the Eocene sandstones in the southern Chindwin Basin, Myanmar: Implications for the unroofing history of the Cretaceous–Eocene magmatic arc: Journal of Asian Earth Sciences, v. 107, p. 172–194, https://doi.org/10.1016/j.jseaes.2015.04.029.

Rogers, J.J.W., and Santosh, M., 2003, Supercontinents in Earth history: Gondwana Research, v. 6, no. 3, p. 357–368, https://doi.org/10.1016/S1342-937X(05)70993-X.

Scherer, E., Munker, C., and Mezger, K., 2001, Calibration of the lutetium-hafnium clock: Science, v. 293, no. 5530, p. 683–687, https://doi.org/10.1126/science.1061372.

Sláma, J., Košler, J., Condon, D.J., Crowley, J.L., Gerdes, A., Hanchar, J.M., Horstwood, M.S.A., Morris, G.A., Nasdala, L., Norberg, N., Schaltegger, U., Schoene, B., Tubrett, M.N., and Whitehouse, M.J., 2008, Plešovice zircon—A new natural reference material for U-Pb and Hf isotopic microanalysis: Chemical Geology, v. 249, no. 1-2, p. 1–35, https://doi.org/10.1016/j.chemgeo.2007.11.005.

Sone, M., and Metcalfe, I., 2008, Parallel Tethyan sutures in mainland Southeast Asia: New insights for Palaeo-Tethys closure and implications for the Indosinian orogeny: Comptes Rendus Geoscience, v. 340, no. 2-3, p. 166–179, https://doi.org/10.1016/j.crte.2007.09.008.

Tran, H.T., Zaw, K., Halpin, J.A., Manaka, T., Meffre, S., Lai, C.-K., Lee, Y., Le, H.V., and Dinh, S., 2014, The Tam Ky-Phuoc Son shear zone in central Vietnam: Tectonic and metallogenic implications: Gondwana Research, v. 26, p. 144–164, https://doi.org/10.1016/j.gr.2013.04.008.

Usuki, T., Lan, C.-Y., Wang, K.-L., and Chiu, H.-Y., 2013, Linking the Indochina block and Gondwana during the early Paleozoic: Evidence from U-Pb ages and Hf isotopes of detrital zircons: Tectonophysics, v. 586, p. 145–159, https://doi.org/10.1016/j.tecto.2012.11.010.

Vervoort, J.D., Patchett, P.J., Söderlund, U., and Baker, M., 2004, Isotopic composition of Yb and the determination of Lu concentrations and Lu/Hf ratios by isotope dilution using MC-ICPMS: Geochemistry Geophysics Geosystems, v. 5, no. 11, Q11002, https://doi.org/10.1029/2004GC000721.

Wang, Q.F., Deng, J., Li, C.S., Li, G.J., Yu, L., and Qiao, L., 2014, The boundary between the Simao and Yangtze blocks and their locations in Gondwana and Rodinia: Constraints from detrital and inherited zircons: Gondwana Research, v. 26, p. 438–448, https://doi.org/10.1016/j.gr.2013.10.002.

Wang, X., and Metcalfe, I., 2000, The Jinshajiang–Ailaoshan suture zone, China: Tectonostratigraphy, age and evolution: Journal of Asian Earth Sciences, v. 18, no. 6, p. 675–690, https://doi.org/10.1016/S1367-9120(00)00039-0.

Wei, Q., and Shen, S., 1997, Arc volcanic rocks of Late Permian (P2) in Taizhong-Lixianjiang zone, Ailao Shan area: Journal of Mineralogy and Petrology, v. 17, p. 8–16.

Wiedenbeck, M., Alle, P., Corfu, F., Griffin, W., Meier, M., Oberli, F., Quadt, A.v., Roddick, J., and Spiegel, W., 1995, Three natural zircon standards for U-Th-Pb, Lu-Hf, trace element and REE analyses: Geostandards Newsletter, v. 19, no. 1, p. 1–23, https://doi.org/10.1111/j.1751-908X.1995.tb00147.x.

Wu, F.-Y., Ji, W.-Q., Liu, C.-Z., and Chung, S.-L., 2010, Detrital zircon U-Pb and Hf isotopic data from the Xigaze fore-arc basin: Constraints on Transhimalayan magmatic evolution in southern Tibet: Chemical Geology, v. 271, no. 1-2, p. 13–25, https://doi.org/10.1016/j.chemgeo.2009.12.007.

Xia, X., Min, S., Geng, H., Sun, Y., Wang, Y., and Zhao, G., 2011, Quasi-simultaneous determination of U-Pb and Hf isotope compositions of zircon by excimer laser-ablation multiple-collector ICPMS: Journal of Analytical Atomic Spectrometry, v. 26, no. 9, p. 1868–1871, https://doi.org/10.1039/c1ja10116a.

Xia, X., Ren, Z., Wei, G., Zhang, L., Sun, M., and Wang, Y., 2013, In situ rutile U-Pb dating by laser ablation MC-ICPMS: Geochemical Journal, v. 47, no. 4, p. 459–468, https://doi.org/10.2343/geochemj.2.0267.

Xia, X., Nie, X., Lai, C.-K., Wang, Y., Long, X., and Meffre, S., 2016, Where was the Ailaoshan Ocean and when did it open: A perspective based on detrital zircon U-Pb age and Hf isotope evidence: Gondwana Research, v. 36, p. 488–502, https://doi.org/10.1016/j.gr.2015.08.006.

Xu, J., Xia, X.-P., Lai, C.-K., Zhou, M., and Ma, P., 2019a, First identification of Late Permian Nb-enriched basalts in Ailaoshan region (SW Yunnan, China): Contribution from Emeishan plume to subduction of eastern Paleotethys: Geophysical Research Letters, v. 46, p. 2511–2523, https://doi.org/10.1029/2018gl081687.

Xu, J., Xia, X., Lai, C., Long, X., and Huang, C., 2019b, When did the Paleotethys Ailaoshan Ocean close: New insights from detrital zircon U-Pb age and Hf isotopes: Tectonics, v. 38, no. 5, p. 1798–1823.

Xu, J., Xia, X., Huang, C., Cai, K., Yin, C., and Lai, C.-K., 2019c, Changes of provenance of Permian and Triassic sedimentary rocks from the Ailaoshan suture zone (SW China) with implications for the closure of the eastern Paleotethys: Journal of Asian Earth Sciences, v. 170, p. 234–248, https://doi.org/10.1016/j.jseaes.2018.10.025.

Xu, L., Lin, Y., Shen, W., Qi, L., Xie, L., and Ouyang, Z., 2007, Platinum-group elements of the Meishan Permian-Triassic boundary section: Evidence for flood basaltic volcanism: Chemical Geology, v. 246, no. 1-2, p. 55–64, https://doi.org/10.1016/j.chemgeo.2007.08.013.

Xu, Y.-G., Luo, Z.-Y., Huang, X.-L., He, B., Xiao, L., Xie, L.-W., and Shi, Y.-R., 2008, Zircon U-Pb and Hf isotope constraints on crustal melting associated with the Emeishan mantle plume: Geochimica et Cosmochimica Acta, v. 72, no. 13, p. 3084–3104, https://doi.org/10.1016/j.gca.2008.04.019.

Yang, J., Cawood, P.A., Du, Y., Huang, H., Huang, H., and Tao, P., 2012, Large igneous province and magmatic arc sourced Permian–Triassic volcanogenic sediments in China: Sedimentary Geology, v. 261–262, p. 120–131, https://doi.org/10.1016/j.sedgeo.2012.03.018.

Yang, L., Wang, Q., Liu, H., Carranza, E.J.M., Li, G., and Zhou, D., 2017, Identification and mapping of geochemical patterns and their significance for regional metallogeny in the southern Sanjiang, China: Ore Geology Reviews, v. 90, p. 1042–1053, https://doi.org/10.1016/j.oregeorev.2016.08.014.

Yang, Q., Xia, X.P., Zhang, W.F., Zhang, Y.Q., Xiong, B.Q., Xu, Y.G., Wang, Q., and Wei, G.J., 2018, An evaluation of precision and accuracy of SIMS oxygen isotope analysis: Solid Earth Sciences, v. 3, p. 81–86, https://doi.org/10.1016/j.sesci.2018.05.001.

Yunnan Bureau of Geology and Mineral Resources (YNGMR), 1990, Regional Geology of Yunnan Province: Beijing, Geological Publishing House, 728 p.

Zaw, K., Meffre, S., Lai, C.K., Burrett, C., Santosh, M., Graham, I., Manaka, T., Salam, A., Kamvong, T., and Cromie, P., 2014, Tectonics and metallogeny of mainland Southeast Asia—A review and contribution: Gondwana Research, v. 26, no. 1, p. 5–30, https://doi.org/10.1016/j.gr.2013.10.010.

Science Editor: Wenjiao Xiao
Associate Editor: Timothy Kusky

Manuscript Received 19 March 2019
Revised Manuscript Received 13 July 2019
Manuscript Accepted 12 August 2019

Printed in the USA